A Fully Nonlinear Numerical Model for Focused Wave Groups

D Z Ning[1], B Teng[1], J Zang[2], S X Liu[1]

[1] State Key Laboratory of Coastal and Offshore Engineering, Dalian University of Technology, Dalian, China
[2] Department of Architecture & Civil Engineering, University of Bath, Bath, UK

e-mail: dzning@dlut.edu.cn, bteng@dlut.edu.cn, j.zang@bath.ac.uk, liusx@dlut.edu.cn

INTRODUCTION

For the safe and economic design of offshore structures in the severe sea environments, accurate models are required for the height, shape and internal flow kinematics of extreme waves. As the largest waves in a random sea state are also irregular and highly nonlinear, it is still a challenging job to accurately describe such a complex problem. Indeed, the study on field data (Rozario, etal, 1993) has shown that the most likely mechanism for the development of extreme waves in a broad-banded sea state results from the focusing of wave energy due to the dispersive nature of the underlying free waves. Therefore, extreme waves do not arise as part of a regular wave train, but occur as individual events at one point in space and time. In this paper we investigate the effect of wave nonlinearity on focusing of localized group of extreme waves using a fully nonlinear numerical scheme based on a higher-order boundary element method (HOBEM).

As an extension of the previous work (Ning and Teng, 2007), the fully nonlinear numerical wave tank is modified to describe the generation and processes of focused wave groups in finite and infinite water depth and capture the instantaneous point at which the extreme wave occurs.

NUMERICAL MODEL

A Cartesian coordinate system is defined with the origin in the plane of the undisturbed free surface, with the z-axis positive upwards. An ideal, irrotational and incompressible fluid is assumed so that a velocity potential $\phi(x, y, z, t)$ exists. The velocity potential $\phi(x, y, z, t)$ satisfies the Laplace equation inside the fluid domain Ω. On the instantaneous free surface, both the fully nonlinear kinematic and dynamic boundary conditions are satisfied. On the solid boundaries (lateral walls and bottom of the tank), the impermeable condition is imposed. At the inflow boundary S_I, the second-order Stokes irregular wave velocity profile along the vertical input boundary are prescribed for the focused wave group, in which the initial phases are chosen to make the velocity largest at the point in the time $t=t_0$ and position $x=x_0$. Meanwhile, the initial calm water surface condition is applied in the present research.

The direct boundary integral equation is derived to solve the prescribed boundary value problem by using the second Green's theorem. Applying the Green function satisfying the impermeable condition on the sea bed and the two lateral walls, the Fredholm integral equation of the second kind can be derived as follows:

$$\alpha(p)\phi(p)-\int_{S_I}\phi(q)\frac{\partial G(p,q)}{\partial n}dS+\int_{S_f}G(p,q)\frac{\partial \phi(q)}{\partial n}dS = -\int_{S_I}G(p,q)\frac{\partial \phi(q)}{\partial n}dS+\int_{S_f}\phi(q)\frac{\partial G(p,q)}{\partial n}dS \quad (1)$$

which only includes the incident boundary and the free surface boundary, where $p=(x_0, y_0, z_0)$ and $q=(x, y, z)$ are source and field points, and $\alpha(p)$ is the solid angle. The Green function can be obtained by the superposition of the image of the Rankine source about the sea bed and the infinite image about the two lateral walls. To ensure the convergence of the Green function, a factor $1/|n|B$ is subtracted from each term (Newman, 1992). The Green function can be written as:

$$G(p,q)=-\frac{1}{4\pi}[G_C(x-x_0,y-y_0,z-z_o)+ G_C(x-x_0,y+y_0,z-z_o)+G_C(x-x_0,y-y_0,z+z_o+2h) +G_C(x-x_0,y+y_0,z+z_o+2h)] \quad (2)$$

where

$$G_C(X,Y,Z)=\frac{1}{\sqrt{X^2+Y^2+Z^2}}+\sum_{n=1}^{\infty}\left(\frac{1}{\sqrt{X^2+(Y+2nB)^2+Z^2}}+\frac{1}{\sqrt{X^2+(Y-2nB)^2+Z^2}}-\frac{1}{nB}\right)$$

where B is the tank width, and h is the water depth. As the lateral walls and the bottom have been eliminated, the present numerical wave tank is easily extended to infinite water depth.

Then the boundary surface is discretized with a

number of elements. The geometry of each element is represented by the shape functions, thus the entire curved boundary can be approximated by a number of higher-order elements. Within the boundary elements, physical variables are also interpolated by the shape functions. The integral equation Eq. 1 can be formulated in the following form

$$\alpha(p)\phi(p)-\sum_{i=1}^{Ne_2}\int_{-1}^{1}\int_{-1}^{1}\sum_{k=1}^{K}h^k(\xi,\varsigma)\phi_k\frac{\partial G(p,q(\xi,\varsigma))}{\partial n}|J(\xi,\varsigma)|d\xi d\varsigma$$
$$+\sum_{i=1}^{Ne_1}\int_{-1}^{1}\int_{-1}^{1}\sum_{k=1}^{K}h^k(\xi,\varsigma)G(p,q(\xi,\varsigma))\frac{\partial\phi_k}{\partial n}|J(\xi,\varsigma)|d\xi d\varsigma$$
$$=-\sum_{i=1}^{Ne_2}\int_{-1}^{1}\int_{-1}^{1}G(p,q(\xi,\varsigma))\frac{\partial\phi(q(\xi,\varsigma))}{\partial n}|J(\xi,\varsigma)|d\xi d\varsigma$$
$$+\sum_{i=1}^{Ne_1}\int_{-1}^{1}\int_{-1}^{1}\frac{\partial G(p,q(\xi,\varsigma))}{\partial n}\phi(q(\xi,\varsigma))|J(\xi,\varsigma)|d\xi d\varsigma \quad (3)$$

in which $J(\xi,\eta)$ represents the Jacobian matrix relating the global coordinate and the local intrinsic coordinates in the i-th element. Ne_1 and Ne_2 are the numbers of the discretized elements on the free surface and the incident surface, respectively. In the integration process, the solid angle, the single layer and double layer integration are directly resolved (Teng, et al, 2006).

Since the discretized integral equation is always variant in time, all the boundary surfaces are regridded and updated at each time step using the semi-mixed Eulerian-Lagrangian scheme and 4th-order Runga-Kutta approach. The influence coefficients are also computed using the updated grids and known values. If the normal velocity on a boundary surface is known, the fluid velocity on the surface can be computed using the following equation

$$\begin{bmatrix}\frac{\partial\phi}{\partial x}\\ \frac{\partial\phi}{\partial y}\\ \frac{\partial\phi}{\partial z}\end{bmatrix}=\begin{bmatrix}\frac{\partial x}{\partial\xi} & \frac{\partial y}{\partial\xi} & \frac{\partial z}{\partial\xi}\\ \frac{\partial x}{\partial\varsigma} & \frac{\partial y}{\partial\varsigma} & \frac{\partial z}{\partial\varsigma}\\ n_x & n_y & n_z\end{bmatrix}^{-1}\begin{bmatrix}\frac{\partial\phi}{\partial\xi}\\ \frac{\partial\phi}{\partial\varsigma}\\ \frac{\partial\phi}{\partial n}\end{bmatrix} \quad (4)$$

where n_x, n_y, n_z are components of the unit normal vector in the x, y and z directions. The particle velocity on the free surface can be obtained correspondingly.

Once the Eq. (3) is solved and all the velocity potentials and their normal derivative in the calculation domain are known, it is easy to obtain the horizontal velocity distribution for any water particle inside the fluid domain from the following equation

$$\frac{\partial\phi(p)}{\partial x}=\int_S\frac{\partial G(p,q)}{\partial x}\frac{\partial\phi(q)}{\partial n}-\phi(q)\frac{\partial}{\partial x}(\frac{\partial G(p,q)}{\partial n})dS \quad (5)$$

LABORATORY EXPERIMENT

The present numerical model has been used to reproduce a physical model test performed in a wave tank ($3m$ x $69m$) at the State Key Laboratory of Coastal and Offshore Engineering, Dalian University of Technology (DUT), China. Experimental data collected from five wave gauges and an acoustic Doppler velocimeter are considered in this paper. The crest/trough focused waves always occur at the gauge 3 by modulating the initial wave phases in the experiments. Fig.1 indicates the experimental arrangement, and Table 1 lists the locations of the wave gauges of interest, relative to the focused position, i.e., gauge 3. The details of the chosen focused wave group analyzed in this paper are given in Table 2. JONSWAP spectrum is used in the experiments. The experimental linearized wave time series can be obtained from the formula $(C-T)/2$, where C means the free surface time history with crest focusing, and T means the free surface with trough focusing. The corresponding spectrum can be obtained using the fast Fourier transform, leading to the result shown in Fig. 2.

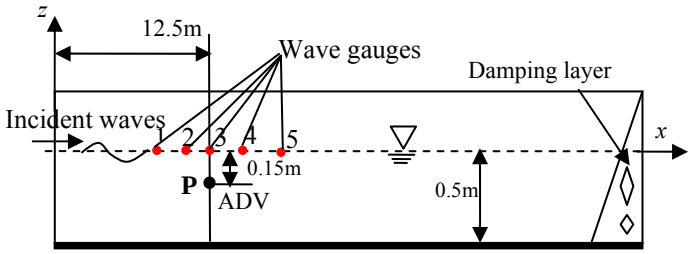

Fig.1 Experimental arrangement

Tab.1 Distances of wave gauges from the No. 3 (m)

d_1	d_2	d_4	d_5
0.99	0.383	0.68	0.88

Tab.2 Input wave group characteristics

Frequency range f (Hz)	$0.6\le f\le 1.5$
Peak frequency f_p	0.80
Incoming wave crest value A_I(m)	0.0875
Wave number N	30
Wave slope ε_i	0.283

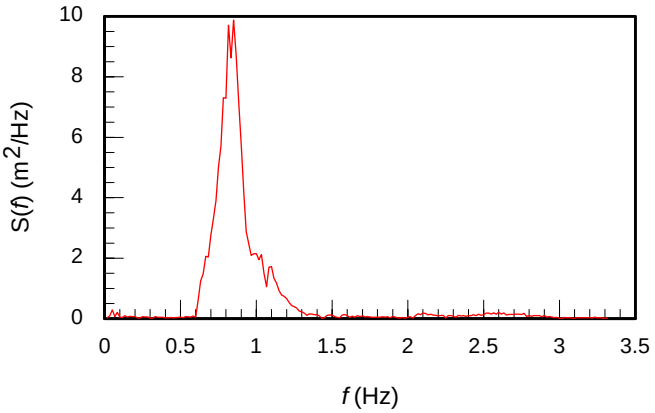

Fig.2 Wave spectrum for linearized incoming wave

NUMERICAL and EXPERIMENTAL RESULTS

In the numerical simulations, wave component with peak frequency f_p is taken as the characteristic wave. The corresponding computational domain is taken as $5\lambda_p \times 0.1\lambda_p$, meshed with 100×2 cells, in which the last $1.5\lambda_p$ is the damping layer. For computing efficiency, the input focus position used for the numerical simulation is chosen at $x_0=1.5\lambda_p$, and the focus time $t_0=6T_p$ (7.5s). Because of wave nonlinearity, the real focal point (x_1 and t_1) is different from the input values and can be found in the numerical simulation based on the NEWWAVE theory.

The comparisons between the numerical simulations and measured data for the crest and trough focused free surface time series at focal point, and the time histories of horizontal velocity at point P are given in Figs.3-6 respectively. For all the results here, the numerical results agree well with the experimental measured data. Numerical results for both crest and trough focused horizontal velocity time histories (with trough focused velocity multiplied by -1) at the focal point on the free surface are given together in Fig.7. The strong nonlinear characteristics are apparently shown in the figure. By using formulas (C-T)/2 and (C+T)/2 for the crest and trough focused velocity time histories, the odd and even harmonics of the horizontal water particle velocity components are obtained as shown in Fig.8. The corresponding spectra of above velocity components can be further obtained using the FFT, as shown in Fig.9. From the figure, the contributions from linear wave, 2nd-order and 3rd-order waves can be seen clearly. Fig.10 concerns the horizontal velocity profile beneath the largest wave crest and the lowest wave trough at the focal point and focal time. Similar phenomena with Bateman et al (2003) are observed.

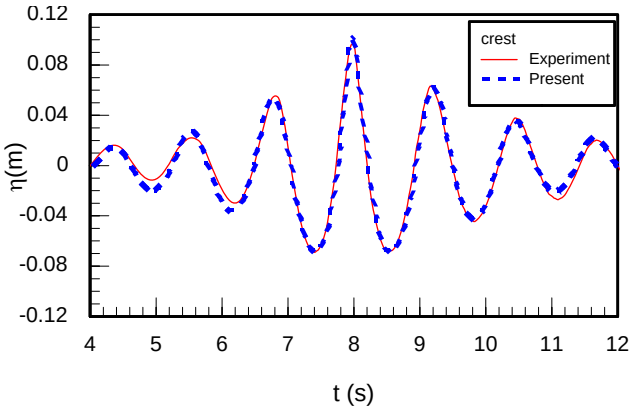

Fig.3 Free surface time series at crest focal point

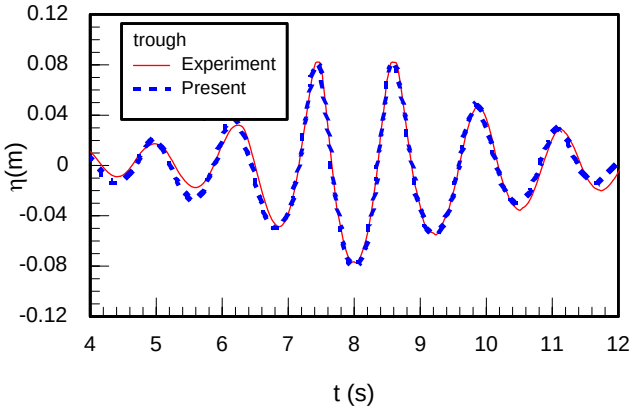

Fig.4 Free surface time series at trough focal point

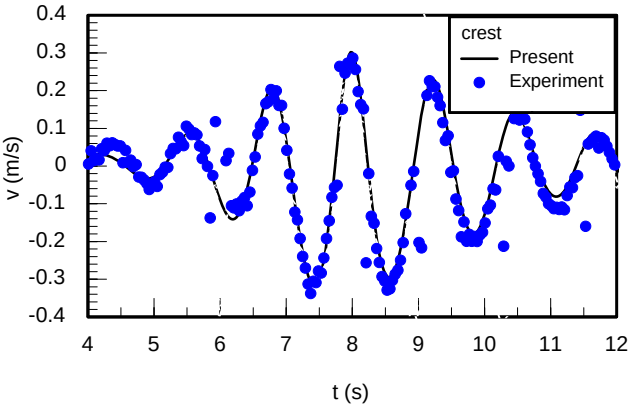

Fig.5 Velocity time histories at crest focal point **P**

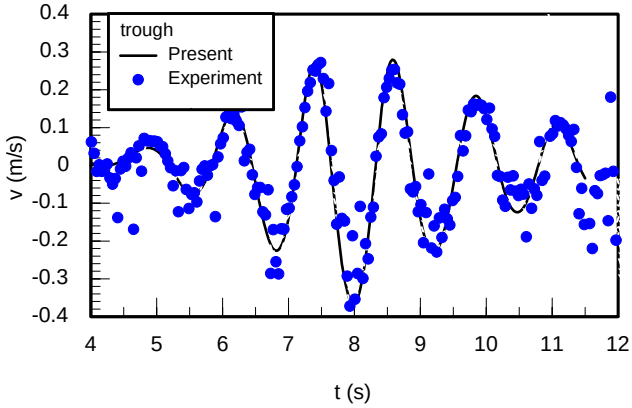

Fig.6 Velocity time histories at trough focal point **P**

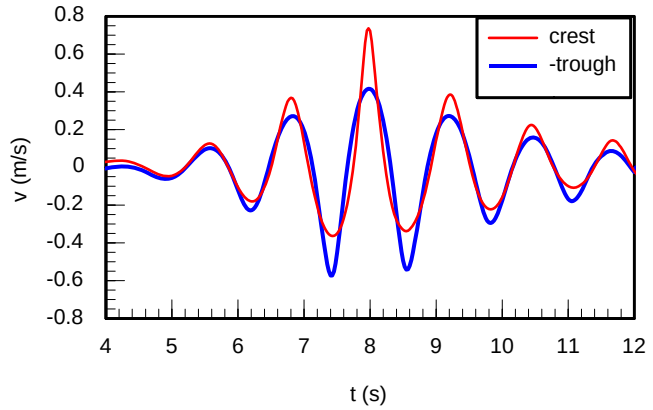

Fig.7 Numerical results for velocity time histories at crest and trough focal point on the free surface

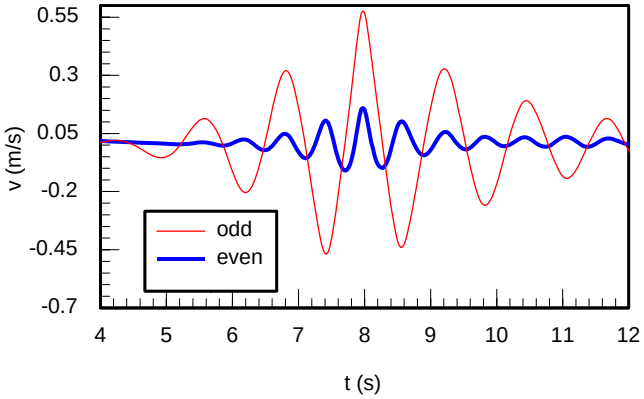

Fig.8 Time histories of crest focal point velocity in odd and even terms on the free surface

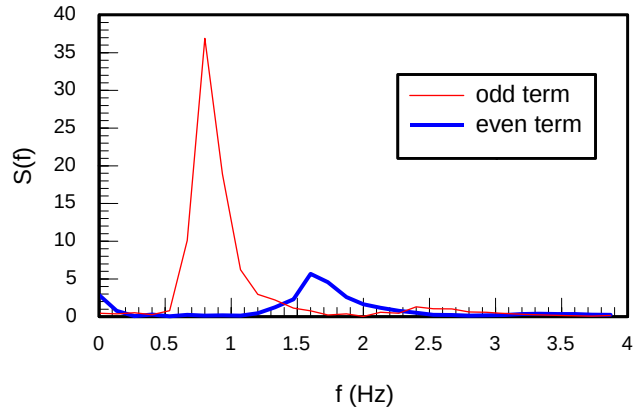

Fig.9 Spectra of crest focused velocities in odd term and even terms

Keeping all unchanged, except extending the water depth to infinite, similar simulations have been carried out. The details of the numerical results and the comparisons with those obtained in finite water depth will be shown in the coming workshop.

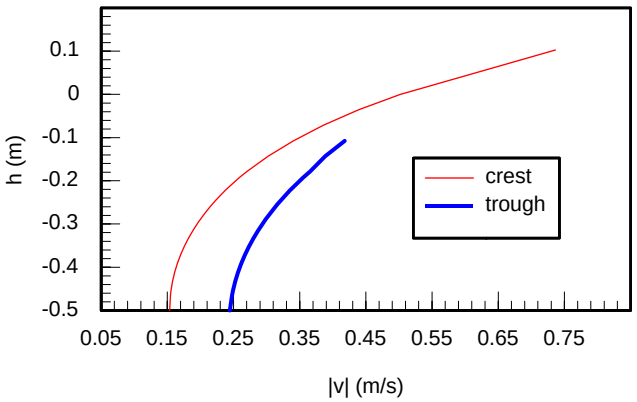

Fig.10 Distribution of largest absolute crest and trough velocities along the water depth

CONCLUSIONS

This paper presents a powerful numerical wave tank for the simulation of focused wave groups both in finite and infinite water depth based on a HOBEM using channel Green function. The results are shown to be accurate and the model is robust. Further examples of wave-structure interaction are ongoing.

ACKNOWLEDGEMENTS

The authors gratefully acknowledge the financial support from China NSFC (Grant Nos. 50709005, 50639030), and UK EPSRC (Grant No GR/T07220/01 and GR/T07220/02).

REFERENCES

Bateman W J D, Swan C and Taylor PH (2003). "On the calculation of the water particle kinematics arising in a directionally spread wavefield." Journal of Computational Physics, 186, pp:70-92.

Rozario JB, Tromans PS, Taylor PH and Efthymiou M (1993). "Comparisons of loads predicted using 'Bew Wave' and other wave models with measurements on Tern structure." In Wave Kinematics and Environmental Forces, Vol. 29. Soc. Underwater Tech., Kluwer, Dordrecht, pp. 143-158.

Ning DZ and Teng B (2007). "Numerical simulation of fully nonlinear irregular wave tank in three dimension." International Journal for Numerical Methods in Fluids, Vol. 43, No. 12, pp. 1847-1862.

Newman J N (1992). "Approximation of free-surface Green functions". In: P. A. Martin & G. R.Whickham (eds), Wave Asympotics. Cambridge University Press, pp. 107-142.

Teng B, Gou Y and Ning DZ (2006). "A Higher Order BEM for Wave-Current Action on Structures—Direct Computation of Free-Term Coefficient and CPV Integrals," China Ocean Engineering.Vol.20, No.3, pp 395-410.